Letter

Severe elastic modulus shift of deformed CoNiCrMo alloy under relative low-temperature exposure

Q. K. Zhang,[1] B. Q. Li,[2] W. X. Li,[1] K. Q. Sun,[1] C. Xu,[1] L. J. Yang,[1] P. Cui,[1] and Z. L. Song[1,*]

[1]*CAS Key Laboratory of Magnetic Materials and Devices, Zhejiang Province Key Laboratory of Magnetic Materials and Application Technology, Ningbo Institute of Materials Technology and Engineering, Chinese Academy of Sciences, Ningbo 315201, People's Republic of China*

[2]*Medtronic Neuromodulation, Fridley, Minnesota 55432, USA*

(Received 18 February 2022; revised 15 September 2022; accepted 9 January 2023; published 19 January 2023)

Elastic modulus (EM) is usually considered to be a relatively stable physical quantity; even phase transformation only results in a little change in EM, while this work demonstrates that it is not so straightforward. Internal friction tests reveal that the EM of a 60% cold-worked CoCrMoNi (MP35N) alloy increases by over 17% after exposed at 100–700 °C, with no change in phase or grains. Analysis of nanoscale structure of the alloy by high-resolution transmission electron microscope shows that high-density nanosized unstable stacking faults and incoherent nanotwins are formed in the cold-worked MP35N alloy, which severely weaken the bonding between the atom planes and decrease the EM. During the exposure process, the unstable fault interfaces and incoherent nanotwins transform into coherent nanotwins or annihilate to decrease the system energy, which repairs the crystal structure and increases the interatomic bonding force and the EM. The segregation of solute atoms at the twin boundaries and stacking faults also contribute a little to the increase in EM. These mechanisms should also suit for the faced centered cubic (FCC)-structured alloys with low-level stacking-fault energy.

DOI: 10.1103/PhysRevB.107.L020102

MP35N, a superalloy containing 35%Ni, 35%Co, 20%Cr, and 10%Mo (wt.%), is widely used for high-strength devices. For these applications, the MP35N usually undergoes a cold-working process followed by exposure at 350 °C to 800 °C. Earlier investigations reveal that tensile strength of the MP35N increases due to the formation of high-density nanotwins during the cold-working and segregation of Mo at the twin boundaries (TBs) and the stacking faults (SFs) occurring during the exposure process [1–5], whereas the elastic modulus (EM) of the MP35N reported from various sources differs greatly [6–8].

The EM, a key parameter for load-bearing devices and construction elements, is commonly considered to be dominated mainly by composition [9]. Besides, due to the anisotropy of EM in the faced centered cubic (FCC) metals, one reason for the change in EM of the polycrystalline is the formation of deformation texture [10]. However, even when a cold-worked MP35N is exposed to a temperature far lower than the recrystallization temperature, its EM still varies with increasing exposure time, with no change in composition, phase, or grains [6,8,10]. Similar phenomena were also observed in some Al alloys, Ti alloys, and nanocrystalline Cu that experienced severe plastic deformation and a relative low-temperature exposure [11–13], which could not be attributed to phase transformation or deformation texture. The micro mechanism requires investigation.

Recent studies reveal the important role of nanotwins and stacking faults on strengthening. Since the grains and phase do not change when the deformed MP35N is exposed to an elevated temperature [6], the effects of recrystallization and phase transformation on the EM changes can be excluded, suggesting that nanotwins and stacking faults may be responsible for the EM variation. In this study, the abnormal EM variation of the MP35N has been measured and the nanoscale microstructure evolution has been characterized. Through analyzing the evolutions of the nanoscale defects, a mechanism of the EM changes has emerged.

The MP35N used in this study was a 60% cold-drawn wire obtained from Fort Wayne Metals with a diameter of 1 mm. An inverted torsion pendulum under a free-damping mode was used to measure the changes in EM [14], with the initial strain amplitude set at 4×10^{-6} of the torsion oscillation [15]. The specimen was heated and cooled between 100 °C to 700 °C with a step of 50 °C (i.e., heated from room temperature to 150 °C, then cooled to room temperature, next heated to 200 °C and cooled, and next to 250 °C). The heating/cooling rate was 10 °C/min. The EM was calculated with the following formula:

$$E = 2(8\pi I l f^2)(1+\mu)/R^4,$$

in which I is the moment of inertia, l is the effective sample length, f is the inherent frequency, R is the sample radius, and μ is the Poisson ratio [16]. To assess the evolution in nanoscale microstructure of the cold-drawn MP35N before and after exposure, some samples were aged at 300 °C and 600 °C for 6 min, and a transmission electron microscope (TEM, JEOL2000FX) was used to characterize the microstructure of the samples cut by focused ion beam.

The real-time increase in EM of the cold-drawn MP35N is shown in Fig. 1, in which the ordinate is the ratio of the EM after each cycle compared to the original value. There

*Corresponding author: songzhenlun@nimte.ac.cn

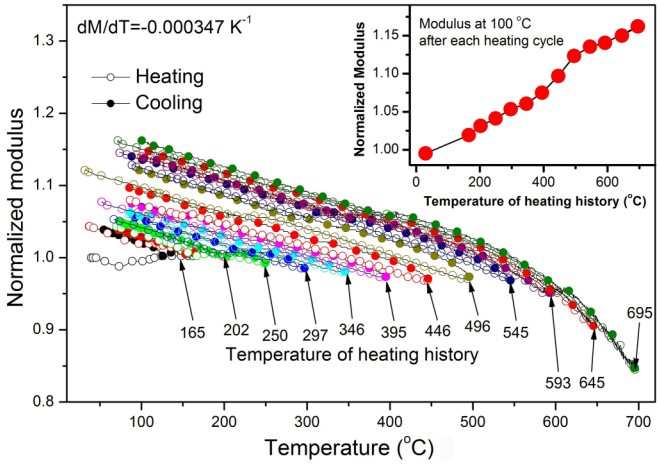

FIG. 1. Modular curves of a 60% cold-drawn MP35N alloy during heating and cooling between 30 °C and 700 °C with a step of about 50 °C.

is obvious increase in EM after each cycle. As presented in the embedded graph, the increase during 400 °C to 550 °C is the fastest, and the total increase is about 17% after heating to 700 °C. These results demonstrate that the activation temperature for the microstructure transformation that increases the EM is very low, and the transformation occurs from room temperature to 700 °C, resulting in a significant increase in EM. Such a change in EM should be a serious consideration in engineering design.

As the phase and grains do not change during the low-temperature exposure process, changes in the nanoscale structure within the grains were characterized by TEM to understand the effects of the exposure, as shown in Fig. 2. For the as-drawn specimen shown in Fig. 2(a), high-density parallel deformation bands can be seen, and the diffraction contrast induced by lattice distortion is obvious at the bands' boundaries. At higher magnification, it was found that the boundaries are sharp TBs or SF interfaces [see Fig. 2(b)]. Since the width of the deformation twins decreases monotonically with decreases in the stacking-fault energy (SFE) [17], and the SFE of the MP35N is very low [18], the twin width is quite thin (2 ∼ 5 nm) and the twin density is very high in the 60% cold-worked MP35N. As reported before, there are both coherent twins and incoherent twins in the deformed FCC alloys [19,20]. In Fig. 2(b), the TBs are mostly incoherent, i.e., there is no common atomic plane for the lattices at the two sides of the TBs, as indicated by the red lines. Although the SFs in Fig. 2(b) are similar to common SFs, the width of the SF interface is obviously higher (∼0.245 nm) than the normal atomic-plane spacing (∼0.193 nm), as marked by "gap" in Fig. 2(b), which indicates a severe lattice distortion and stress field around the SF interface. According to the Lennard-Jones interatomic potential, it is predicated that the wider atomic-plane spacing will decrease the attractive force between the atomic planes at the SF interfaces. The incoherent TB and SF are both incoherent and two-dimensional defects, and the incoherent twin can be considered to be a coherent twin with SF, they can be collectively referred to as "ITBSF." As nan plane defects in the crystal, the very high-density ITBSF

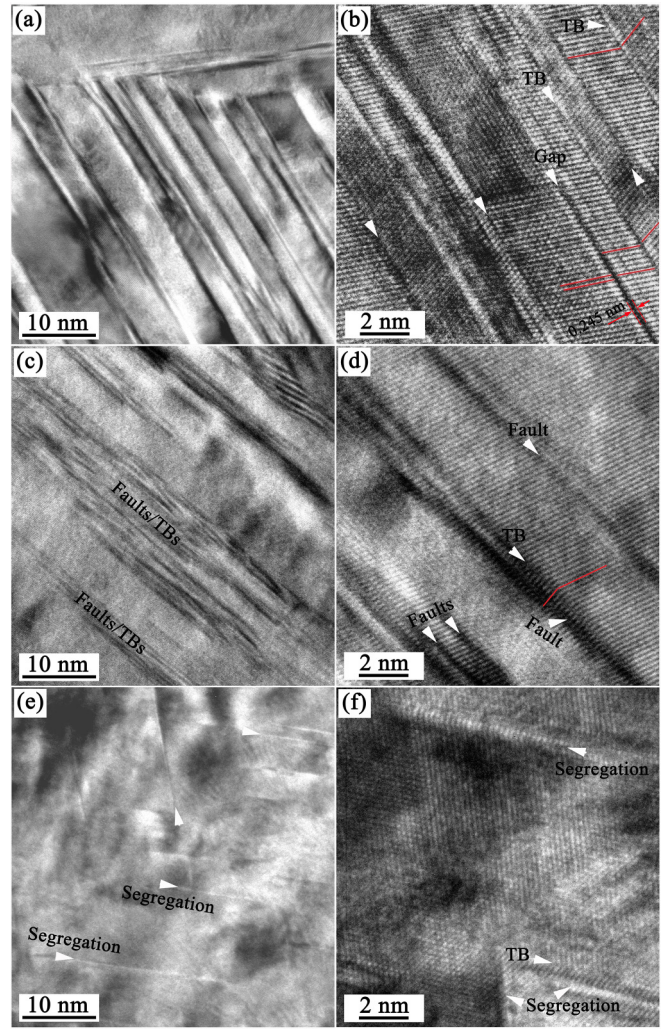

FIG. 2. Microstructures of the MP35N alloy: (a), (b) after 60% cold drawn; (c), (d) aged at 300 °C for 6 min after the cold-working; and (e), (f) aged at 600 °C for 6 min after the cold-working.

will weaken the bonding between the atomic planes. With further deformation, these ITBSF will transform into new grain boundaries or microcracks [21–23]. Since the distortion at the ITBSF is much higher than that at the coherent TBs, these incoherent defects locate at high-energy state and are unstable [19]. After aged at 300 °C for 6 min, the deformation bands can still be identified, as presented in Fig. 2(c), whereas fewer TBs and SFs were found in the high-resolution image [Fig. 2(d)], and the TBs or SF interfaces are not as sharp as that in Fig. 2(b), i.e., the interfacial lattice distortion at the ITBSF is less serious. Therefore, it can be assumed that some of the ITBSF have disappeared or become less incoherent. After aging at 600 °C, the ITBSF have almost disappeared, and some thin and bright bands were identified, as indicated by the arrows in Fig. 2(e). Figure 2(f) reveals that there are thin bands localized around the TBs or SF interfaces. As the bright region corresponds to the concentration of heavier elements, formation of these bands is attributed to the segregation of Mo and Cr atoms [6,24,25]. The TEM images reveal that after a short-term exposure, obvious transformation occurs at the ITBSF to release the lattice distortion, resulting in nanoscale

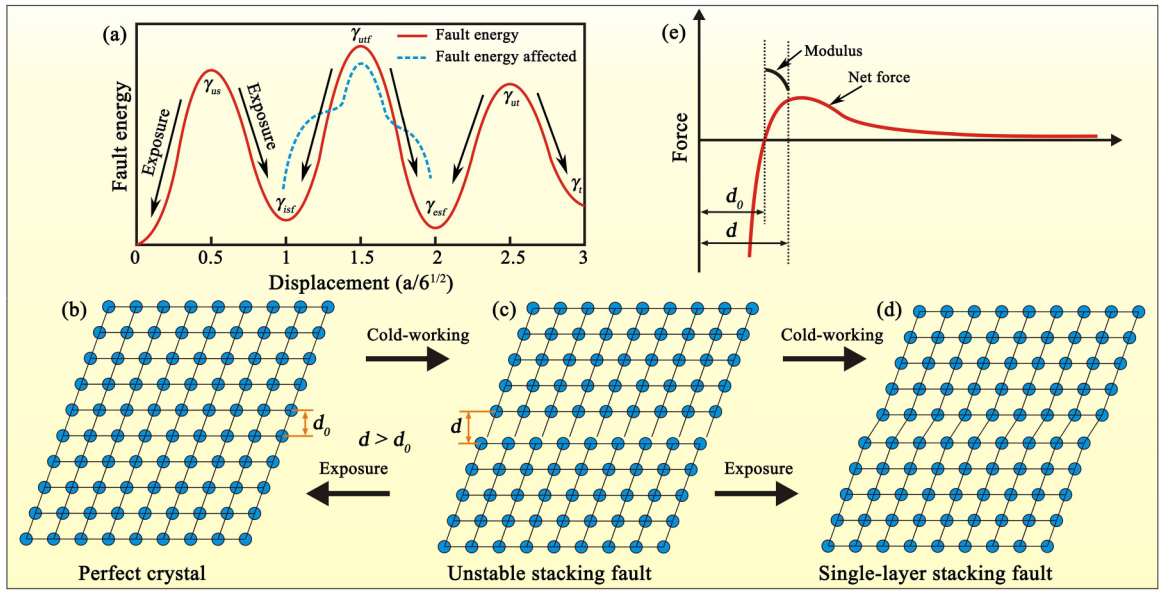

FIG. 3. Illustrations on evolution of the unstable fault during the cold-working and exposure processes: (a) typical generalized planar fault-energy curve for an FCC metal, γ_{us} is the unstable stacking fault energy, γ_{isf} is the intrinsic stacking-fault energy, γ_{utf} is the unstable twin-fault energy, γ_{esf} is the extrinsic stacking-fault energy, γ_{ut} is the energy barrier for the formation of a three-layer twin, γ_t is the twin energy; atomic configurations of (b) perfect crystal; (c) unstable stacking fault; (d) intrinsic stacking fault; and (e) dependence of interatomic force and modulus based on Lennard-Jones potential.

partial recovery, and some solute elements segregate at the TBs and SF interfaces when the exposure temperature is increased. As the grains and phase do not change, this microstructure evolution and segregation may be the reason for the obvious increase in EM.

As shown in Fig. 2, the incoherent TBs and faults disappear or transform after the exposure, which leads to additional research focus on clarifying their evolution mechanisms. During the cold-working process, high-density twins and SFs can be formed in the FCC-structured metals [19,26–29]. *In situ* observation on deformation of the FCC metals reveals that formation and elimination of the SFs and twins occurs dynamically [30,31]. When a stress is applied on the FCC crystal, glide of a Shockley partial on a {111} plane will form a single-layer SF named "intrinsic stacking fault," and glide of an identical partial on an adjacent {111} plane forms a two-layer fault named "extrinsic stacking fault" or "twin fault" [19,28,29]. With gliding of more identical partials on the adjacent planes, twins of three or more layers will be formed. There are also intermediate states between the perfect crystal, single-layer SF, two-layer fault, and so on, called "unstable stacking faults," "unstable twin faults," and "unstable twins," respectively [32]. During the formation processes of the twins and SFs, a series of energy barriers must be overcome [28,29,32], as shown in Fig. 3(a). As formation of the SFs and twins is continuous, the high-energy intermediate states, such as unstable SFs and unstable twins, can be reached under the applied stress [31], while the strain energy stored in the lattice around these microdefects can promote the evolution of microdefects [33], whereas since the plastic deformation contributed by the SF and nanotwins cannot recover immediately once the specimen is unloaded, these unstable microdefects should not transform immediately after unloading. Although thermodynamically a single unstable fault cannot exist, it is possible for a group of unstable faults or TBs to interact with each other and achieve a metastable state, if the distortion stress field of these adjacent unstable defects can maintain a balance [34], which is similar to tripod legs supporting each other. There should be some discrepancy between simulations and experiments on the twinning propensity of the FCC metals [35], and the modeling and calculation may be optimized by considering the interaction of the microdefects. A possible energy curve of a fault considering the surrounding microdefects is illustrated by the dotted line in Fig. 3(a), in which energy platforms exist. Moreover, unstable deformation twins have also been observed in the pure Al and W at low exposure temperature [36,37].

Figures 3(b)–3(d) illustrate the evolution of the unstable one-layer fault during the cold-working and exposure processes based on the TEM observation. During the cold-working process, glide of the atomic plane forms the unstable fault and then a one-layer fault. The atomic-plane spacing at the unstable fault interface (d) is larger than the normal atomic-plane spacing (d_0). When a SF is formed, the atomic bonding between the atomic planes at the SF interface will be weakened, especially at the unstable SF interface. On macrolevel, the weakened bonding force is exhibited as a decrease in EM. In fact, decrease in EM of graphene induced by presence of lattice defects has been proved [38]. When the unstable faults transform into a stable one-layer fault, the atomic-plane spacing becomes close to normal [see Fig. 3(d)], and the atomic bonding can recover. According to the fault-energy curve, if the cold-working is stopped before an unstable fault transforms into a one-layer fault, the unstable fault may transform into perfect crystal or one-layer fault to decrease the energy. Transformation of an incoherent TB should exhibit a similar process. As the loading condition of each atom in an atomic plane is the same, the interaction

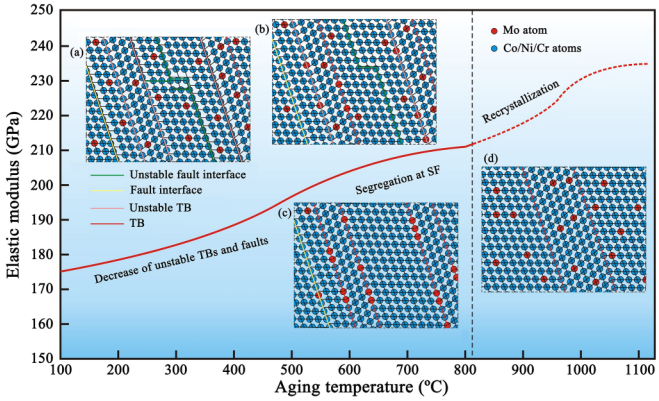

FIG. 4. Illustrations of the increase in EM and inner-crystal microstructure evolution of the cold-worked MP35N during the exposure process; the insets shows the atomic arrangement at nanoscale: (a) cold-worked, exposed at relative (b) low and high (c) temperature before recrystallization; and (d) recrystallized crystal.

force between the two atomic planes at the two sides of the twin-fault interface can be simplified to the force between two atoms. According to the Lennard-Jones potential, there is a balance distance, d_0, between the two atoms. Figure 3(e) qualitatively illustrates the distance dependence of the bonding force and the modulus between the atomic planes. The modulus, as the slope of the net force curve, decreases when the distance (d) is larger than d_0. As the atomic-plane spacing is increased when lattice distortion occur, the attractive force will decrease. During the exposure process, the atomic-plane spacing at the ITBSF gradually returns to the balance distance and the EM recovers.

The evolution in EM of the cold-worked MP35N with increasing exposure temperature is shown in Fig. 4. First, the increase in GBs, TBs, and SFs during the cold-working will destroy the perfect crystal, forming high-density two-dimensional defects, which weaken the atomic bonding and decrease the EM, as exhibited in Fig. 4(a). During the elevated temperature (<700 °C) exposure process, there is no change in grain structure, while the ITBSF disappear or gradually transform into coherent interfaces [see Figs. 4(b) and 4(c)]. In fact, Electron Backscatter Diffraction (EBSD) analysis has revealed that the density of the coherent twins in the cold-worked MP35N increases after exposure [39]. As a result, the distortion at the coherent interfaces is reduced and the atomic-plane spacing returns back to normal, repairing the atomic bonding and recovering the EM. Because the incoherent twins and unstable faults are in high-energy state, these transformations are thermodynamically favored, and their evolutionary mechanism is small-scaled atomic motion rather than long-range diffusion and thus can occur even at very low temperatures [30,37]. Since the Mo atoms segregate at the SFs of the aged MP35N [6,24,25], and the bonding energy between the Mo atoms is higher than that between the Mo atoms and the other three atoms [40], the Mo segregation will also increase the EM. However, the contribution of segregation to the increase in EM was estimated to be very low, because the atomic percentage of Mo is only 6%. Even if all the Mo atoms segregate from complete dispersion, the resulting increase in EM is estimated to be lower, 5%. In fact, the segregation is actually an increase in the ratio of Mo atoms around the faults rather than fully segregation [24,25,41,42]. When the cold-worked MP35N is exposed at a temperature lower than 800 °C, the growth rate of the EM initially increases and then decreases, due to elimination of the ITBSF and the segregation reaching its peak at 400 °C–500 °C. When the exposure temperature is higher than 800 °C, dislocation cancellation and recrystallization will further repair the crystal and recover the EM [8], as in Fig. 4(d).

Since the decrease in EM is induced by the high-density unstable faults and incoherent nanotwins, similar decrease and recovery of the EM should also exist in some other FCC alloys, if high-density nanoscale defects are formed during cold-working, and vice versa for the evolution after thermal exposure. It is important to note the change in EM induced by nanoscale structure evolution in structural design. In the cases of high-SF energy materials, the density of SF is relatively low in the deformed materials and its effect on the EM maybe less obvious. Nevertheless, single-phase alloys such as high-entropy alloys may exhibit this effect more significantly since the other factors affecting the EM can be excluded. The recovery of the unstable SFs and nanotwins in some other alloys such as Cu alloy may occur within a very short time after unloading and usually not be noticed.

In summary, we propose that the reason for the significant decrease in EM of the heavily cold-worked MP35N is the formation of high-density incoherent twins and unstable SFs, which obviously weaken the atomic bonding. When the cold-worked MP35N is exposed at an elevated temperature, these incoherent TBs and unstable SFs annihilate or transform into more stable interfaces due to reconfiguration, which reduces the crystal lattice distortion and increases the bonding force and the EM. It is noted that this transformation does not lead to a change in the phase or grain in the micrometer level. Our findings also suggests this mechanism can be further applied to similar alloys and this effect should be seriously considered in engineering designs.

[1] A. Ishmaku and K. Han, Deformation induced nanostructure and texture in MP35N alloys, J. Mater. Sci. **39**, 5417 (2004).

[2] S. Asgari, E. El-Danaf, E. Shaji, S. R. Kalidindi, and R. D. Doherty, The secondary hardening phenomenon in strain-hardened MP35N alloy, Acta Mater. **46**, 5795 (1998).

[3] S. Asgari, Anomalous plastic behavior of fine-grained MP35N alloy during room temperature tensile testing, J. Mater. Process. Tech. **155-156**, 1905 (2004).

[4] A. Ishmaku and K. Han, Characterization of cold-rolled and aged MP35N alloys, Mater. Charact. **47**, 139 (2001).

[5] M. J. N. V. Prasad, M. W. Reiterer, and K. S. Kumar, Microstructure and mechanical behavior of an as-drawn MP35N alloy wire, Mater. Sci. Eng. A **610**, 326 (2014).

[6] D. Sorensen, B. Q. Li, W. W. Gerberich, and K. A. Mkhoyan, Investigation of secondary hardening in Co-35Ni-20Cr-10Mo

alloy using analytical scanning transmission electron microscopy, Acta Mater. **63**, 63 (2014).
[7] T. Otomo, H. Matsumoto, N. Nomura, and A. Chiba, Influence of cold-working and subsequent heat-treatment on Young's modulus and strength of Co-Ni-Cr-Mo alloy, Mater. Trans. **51**, 434 (2010).
[8] M. J. N. V. Prasad, M. W. Reiterer, and K. S. Kumar, Microstructure and mechanical behavior of annealed MP35N alloy wire, Mater. Sci. Eng. A **636**, 340 (2015).
[9] M. A. Meyers and K. K. Chawla, *Mechanical Behavior of Materials*, 2nd ed. (Cambridge University Press, London, 2009).
[10] B. Q. Li and T. Steigauf, Crystallography Texture and Mechanical Properties of MP35N Wire, Materials Processes for Medical Devices Conference, ASM. September 23–25, Palm Desert, California, 2007.
[11] G. Abrosimova, A. Aronin, D. Fokin, N. Orlova, and E. Postnova, The decrease of Young's modulus in shear bands of amorphous $Al_{87}Ni_8La$ alloy after deformation, Mater. Lett. **252**, 114 (2019).
[12] Y. Lv, Z. Ding, J. Xue, G. Sha, E. Lu, L. Wang, W. Lu, C. Su, and L. C. Zhang, Deformation mechanisms in surface nanocrystallization of low elastic modulus Ti6Al4V/Zn composite during severe plastic deformation, Scr. Mater. **157**, 142 (2018).
[13] M. Zhang, K. Sun, and L. Fang, Influence of grain boundary activites on elastic and plastic deformation of nanocrystalline Cu as studied by phase field and atomistic simulation, Int. J. Mech. Sci. **187**, 105911 (2020).
[14] T. S. Ke, Experimental evidence of the viscous behavior of grain boundaries in metals, Phys. Rev. **71**, 533 (1947).
[15] C. J. Nederveen and C. W. van der Wal, A torsion pendulum for the determination of shear modulus and damping around 1 Hz, Rheol. Acta **6**, 316 (1967).
[16] D. B. Liu, Y. M. He, P. Hu, Z. P. Gan, and H. M. Ding, A modified torsion pendulum for measuring the shear modulus of a single micro-sized filament, Acta. Mech. Solida Sin. **27**, 221 (2014).
[17] Y. Zhang, N. R. Tao, and K. Lu, Effect of stacking-fault energy on deformation twin thickness in Cu-Al alloys, Scr. Mater. **60**, 211 (2009).
[18] E. El-Danaf, S. R. Kalidindi, and R. D. Doherty, Influence of deformation path on the tensile hardening behavior and microstructure evolution in low SFE FCC metals, Int. J. Plast. **17**, 1245 (2001).
[19] I. J. Beyerlein, X. H. Zhang, and A. Misra, Growth twins and deformation twins in metals, Annu. Rev. Mater. Res. **44**, 329 (2014).
[20] N. Li, J. Wang, Y. Q. Wang, Y. Serruys, M. Nastasi, and A. Misra, Incoherent twin boundary migration induced by ion irradiation in Cu, J. Appl. Phys. **113**, 023508 (2013).
[21] C. Blochwitz and W. Tirschler, Twin boundaries as crack nucleation sites, Cryst. Res. Technol. **40**, 32 (2005).
[22] Y. B. Wang, X. Z. Liao, Y. H. Zhao, E. J. Lavernia, S. P. Ringer, Z. Horita, T. G. Langdon, and Y. T. Zhu, The role of stacking faults and twin boundaries in grain refinement of a Cu-Zn alloy processed by high-pressure torsion, Mater. Sci. Eng. A **527**, 4959 (2010).
[23] L. L. Li, Z. J. Zhang, P. Zhang, Z. G. Wang, and Z. F. Zhang, Controllable fatigue cracking mechanisms of copper bicrystals with a coherent twin boundary, Nat Commun. **5**, 3536 (2014).
[24] S. Antonov, B. Li, B. Gault, and Q. Tan, The effect of solute segregation to deformation twin boundaries on the electrical resistivity of a single-phase superalloy, Scr. Mater. **186**, 208 (2020).
[25] G. W. Han, I. P. Jones, and R. E. Smallman, Direct evidence for Suzuki segregation and Cottrell pinning in MP159 superalloy obtained by FEG(S)TEM/EDX, Acta Mater. **51**, 2731 (2003).
[26] J. W. Christian and S. Mahajan, Deformation twinning, Prog. Mater. Sci. **39**, 1 (1995).
[27] L. G. Sun, X. Q. He, and J. Lu, Nanotwinned and hierarchical nanotwinned metals: A review of experimental, computational and theoretical efforts, npj Comput. Mater. **4**, 6 (2018).
[28] S. Y. Hu, C. H. Henager, Jr., and L. Q. Chen, Simulations of stress-induced twinning and de-twinning: A phase field model, Acta Mater. **58**, 6554 (2010).
[29] Z. J. Zhang, H. W. Sheng, Z. J. Wang, B. Gludovatz, Z. Zhang, E. P. George, Q. Yu, S. X. Mao, and R. O. Ritchie, Dislocation mechanisms and 3D twin architectures generate exceptional strength-ductility-toughness combination in CrCoNi medium-entropy alloy, Nat Commun. **8**, 14390 (2017).
[30] L. H. Wang, Z. Zhang, and X. D. Han, In situ experimental mechanics of nanomaterials at the atomic scale, NPG Asia Mater. **5**, e40 (2013).
[31] L. H. Wang, P. F. Guan, J. Teng, P. Liu, D. K. Chen, W. Y. Xie, D. L. Kong, S. B. Zhang, T. Zhu, Z. Zhang, E. Ma, M. W. Chen, and X. D. Han, New twinning route in face-centered cubic nanocrystalline metals, Nat Commun. **8**, 2142 (2017).
[32] Y. T. Zhu, X. Z. Liao, and X. L. Wu, Deformation twinning in nanocrystalline materials, Prog. Mater. Sci. **57**, 1 (2012).
[33] J. C. Nieto-Fuentes, S. Osovski, A. Venkert, and D. Rittel, Reassessment of the Dynamic Thermomechanical Conversion in Metals, Phys. Rev. Lett. **123**, 255502 (2019).
[34] G. Schoeck, The interaction of dislocations and planar faults in solids, Philos. Mag. Lett. **69**, 131 (1994).
[35] X. L. Wu and Y. T. Zhu, Inverse Grain-Size Effect on Twinning in Nanocrystalline Ni, Phys. Rev. Lett. **101**, 025503 (2008).
[36] B. Q. Li, M. L. Sui, B. Li, E. Ma, and S. X. Mao, Reversible Twinning in Pure Aluminum, Phys. Rev. Lett. **102**, 205504 (2009).
[37] X. Wang, J. W. Wang, Y. He, C. M. Wang, L. Zhong, and S. X. Mao, Unstable twin in body-centered cubic tungsten nanocrystals, Nat Commun. **11**, 2497 (2020).
[38] H. Mizuno, L. E. Silbert, and M. Sperl, Spatial Distributions of Local Elastic Moduli near the Jamming Transition, Phys. Rev. Lett. **116**, 068302 (2016).
[39] Heat Treatment Effect on CSL Boundary in MP35N, Document No. NRP0001-50948, Medtronic MRCS.
[40] J. X. Li, K. Yamanaka, and A. Chiba, Influence of interatomic interactions on the mechanical properties of face-centered cubic multicomponent Co-Ni-Cr-Mo alloys, Materialia **12**, 100742 (2020).
[41] D. Sorensen, B. Q. Li, W. W. Gerberich, and K. A. Mkhoyan, Investigation of secondary hardening in MP35N wires, Microsc. Microanal. **19** (Suppl 2), 1778 (2013).
[42] S. Q. Lu, B. Z. Shang, Z. J. Luo, R. H. Wang, and F. C. Zeng, The effect of the thermal exposure on microstructure of MP159 alloy, J. Mater. Sci. **34**, 5449 (1999).